Directionality Control of Light-emitting Devices through Sub-micron Dielectric Structures

Yoshikuni Hirano, Katsu Tanaka, Yasushi Motoyama, Nobuo Saito
and Hiroshi Kikuchiand Naoki Shimidzu
Science & Technology Research Laboratories, NHK (Japan Broadcasting Corporation),
1-10-11 Kinuta, Setagaya-ku, Tokyo, Japan

Keywords: Light-emitting Diodes, Directionality Control, Direct-view-Type Display.

Abstract: We have been investigating directional light control methods of light-emitting diodes (LEDs). We propose a method that makes it possible to control a principal axis in field intensity through fine-structures on the LEDs. We also describe the concept of this method and essential points for obtaining a sharply defined principal axis. The effectiveness of the method was verified through differences in angular distributions by using the finite-different time-domain method.

1 INTRODUCTION

Light emitting diodes (LEDs) are expected to be a next generation light source and have been applied to many lighting applications, such as general lighting (Krames, 2007), visible-light communication (McKendry, 2012), and displays (Day, 2011) due to advances in high-brightness technology. Because of the Lambertian pattern in the spatial intensity distribution of an LED, the direct-view-type display, which consists of as many fine LED chips as the number of pixels, has wider viewing angles (Sony corp., 2012).

The Lambertian pattern is not suitable for certain applications, and the directionality control of LEDs has been studied for mainly narrowing the angular distribution. In an automotive lighting area, for example, the sharper angular distribution will enable the lighting of a restricted region and reduce blinding glare from oncoming vehicles (Krames, 2007). In projection display systems, light use efficiency is improved by increasing the incident light flux from a light source to projection optics (Fournier, 2008). In addition to the modifying angular distribution of LEDs, new applications will be possible if off-axis directionality control becomes possible.

Projection optics for modifying the far-field pattern of an LED is also important to downsize projection display systems (Tu, 2009). Recently, several directional light control methods have been proposed for LEDs with photonic crystals (McGroddy, 2008). For instance, the angular distribution of the directional light at half intensity near 66º from a 5-μm aperture was demonstrated in an experiment with a prototype of GaN-based LEDs with photonic crystals (Lai, 2012). This result indicates that increasing light emission in useful directions eliminates the need for some optical elements to concentrate the emission light from an LED into projection optics. The directional light control method enables a projector to be small, light weight, and exhibit high definition. In addition, the off-axis directionality control reduces the projection optics and allows more compact projection systems. However, more complex designed crystal lattice and excessive lattice points are necessary to achieve sharply defined off-axis directional light beam.

Off-axis directionality control allows high picture quality technology for auto-stereoscopic three-dimensional (3D) multi-view displays (Son, 2010). Several types of 3D displays produce 3D images by using many directional lights using a multi-projector, parallax barrier, and lens array. The ideal 3D display requires a number of directional lights across the entire viewing space. Therefore, a high-density array of an off-axis directionality-controlled light emitting device is useful for such 3D displays. More recently, multi-directional backlight technology has been proposed to provide high-

Hirano Y., Tanaka K., Motoyama Y., Saito N., Kikuchi H. and Shimidzu N..
Directionality Control of Light-emitting Devices through Sub-micron Dielectric Structures.
DOI: 10.5220/0004698701630169
In *Proceedings of 2nd International Conference on Photonics, Optics and Laser Technology* (PHOTOPTICS-2014), pages 163-169
ISBN: 978-989-758-008-6

resolution, full-parallax 3D images by using an optical grating (Fattal, 2013). Fattal et al. introduced the directional control method for an LED using a number of 10-μm optical gratings having various directions. They then fabricated a 64-view backlight and produced 3D images with a spatial resolution of 88 pixels per inch and full-motion parallax. However, because of the reduction of undesirable lights, the device size is un-diminishable and this method is not suitable for high-density array devices.

In this study, we propose a method for controlling the off-axis directionality control of LEDs, which is suitable for high-density array devices. In the method, a control unit, which consists of several sub-micron dielectric structures, is placed on the light emitting surface and the tops of these structures function as apertures. The control unit provides a directional light, called a principal axis, by the diffraction of light from the apertures. The principal axis direction depends on the phase difference at the apertures and is controlled by the difference in the height of the sub-micron dielectric structures h.

We also describe the design rules of the sub-micron dielectric structures' dimensions and arrangements for controlling directional light. We also describe the essential points for obtaining a sharply defined principal axis. The effects of the proposed method were verified through directionality control characteristics in one control unit by using the finite-different time-domain (FDTD) method.

2 BASIC STRUCTURE

2.1 Directionality Control Method

Multiple control units on an LED surface are shown in Figure 1(a). A control unit manipulates a principal axis toward a different direction. A single control unit (Figure 1(b)) consists of cylinders of w in diameter, where w is the length divided by the center wavelength λ of the LED. In this section, we describe the dimensions in units of λ, unless otherwise stated. The cylindrical structures A, B, and C on an LED surface and the LED are of the same material of a refractive index n ($n > 1$). Heights of structures A and B are denoted as b and that of structure C is b - h in height. The structures are placed on a vertex of a regular triangle p on a side, which means their gaps are p - w. We use a system of coordinates with their origin at the center of the control units on the plane containing the tops of structures A and B. The z-axis is perpendicular to the LED surface, then the principal axis contains the z-axis when h = 0. The x-axis is parallel to the line from the origin to the midpoint of the center points of structures A and B. In addition, ϕ and θ are the horizontal and zenithal angle, as shown in Figure 2.

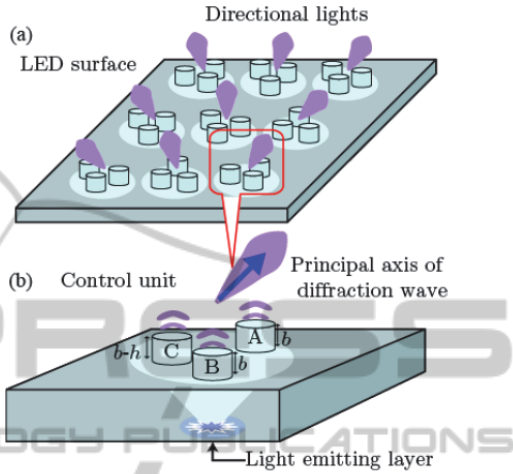

Figure 1: Schematics of (a) device with proposed method and (b) directionality control unit in device array. Control unit consists of three cylindrical structures A, B and C. Lights from light emitting layer enter from bottom of each structure and exits from their tops. Optical path lengths via each structure depend on height of structures. Principal axis, defined as direction of optical path differences via all structures equal to zero, is controlled by difference in height of structures h.

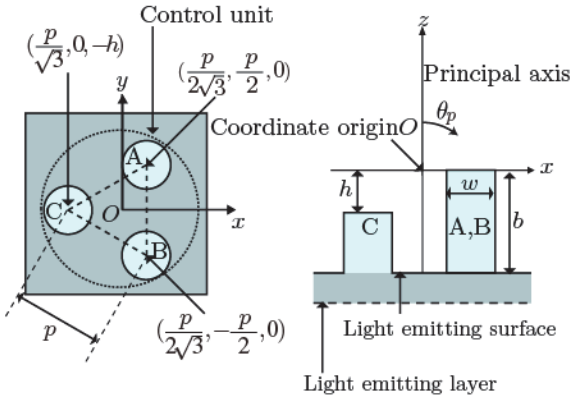

Figure 2: Top view and cross-sectional diagram on vertical plane including x-axis of control unit. Cartesian coordinate system is used with their origin at center of tops of structures at h = 0. Z-axis is perpendicular to light emitting surface and x-axis is parallel to line from origin to midpoint of center points of structures A and B.

Multiple lights, which are emitted from the tops of the structures in phase, form a diffraction pattern,

like hexagonally arranged spots in an image plane. For simplicity, we assume that incident light is in phase at the bottoms of the structures. The center spot in the diffraction pattern corresponds to a principal axis, whose direction is determined as that where all of the optical path lengths from the bottoms of the structures to the image plane are equal.

If h is not equal to 0, the optical path length from the bottom to the top of structure C is nh shorter than those of structures A and B. The distance from the top of structure C to the image plane is longer than those from the tops of structures A and B. Because the structures' arrangements are in symmetry with the xz-plane, the principal axis direction is denoted as θ_p. We define a plane S, which is perpendicular to the xz-plane and at a distance of l from the original point, as the image plane, as shown in Figure 3. Optical paths l_a, l_b, and l_c from the bottoms of structures A, B, and C to S by way of the tops of the structures are expressed as

$$l_a = l_b = l - \frac{1}{2\sqrt{3}} p \sin\theta_p + nb \tag{1}$$

$$l_c = l + \frac{1}{\sqrt{3}} p \sin\theta_p + h\cos\theta_p + n(b-h) \tag{2}$$

Then the difference in optical path lengths between l_a, l_b, and l_c are expressed as

$$l_c - l_{a,b} = \frac{\sqrt{3}}{2} p \sin\theta_p + h\cos\theta_p - nh = m\lambda \tag{3}$$

Here, m is the optical path difference between the lengths of l_a, l_b, and l_c. The θ_p of an m-th order diffraction wave on the vertical plane including the x-axis can be obtained by solving Equation (3).

$$\theta_p = \sin^{-1} \frac{nq + 2m\lambda/\sqrt{3}p}{\sqrt{1+q^2}} - \tan^{-1} q \tag{4}$$

Here,

$$q = \frac{2h}{\sqrt{3}p} \tag{5}$$

When we assume that the principal axis direction is given by Equation (1) at m = 0, θ_p depends on parameter q, and monotonically increases within the following range.

$$0 \le q \le 1/\sqrt{n^2-1} \tag{6}$$

However, the maximum angle of the principal axis θ_p is given by Equation (7), which depends only on the index.

$$\theta_p \le \tan^{-1} \sqrt{n^2-1} \tag{7}$$

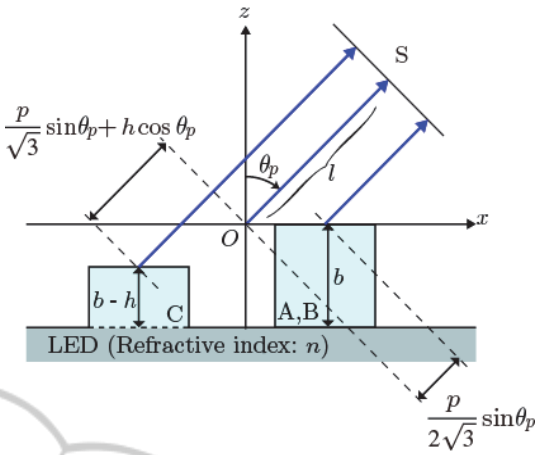

Figure 3: Principal axis direction on vertical plane including x-axis. Image plane S is l in shortest distance from origin point and θ_p in angle formed by l and z-axis.

Therefore the maximum value of θ_p is constrained by the structures' dimensions. A principal axis should be made within the airly patterns of the structures. The θ_p is restricted to the following range.

$$\theta_p \le \sin^{-1} \frac{1.22}{w} \tag{8}$$

Too small of structure gaps p - w confine the working range of θ_p. The gap and h should satisfy the following equation to prevent an obstruction in the line of sight along the x-axis from the top of structure C by another structure.

$$\theta_p \le \tan^{-1} \frac{p-w}{h} \tag{9}$$

Regarding the y-direction, we use the following condition to prevent light scattering by another structure.

$$p > w/\cos\frac{\pi}{6} \tag{10}$$

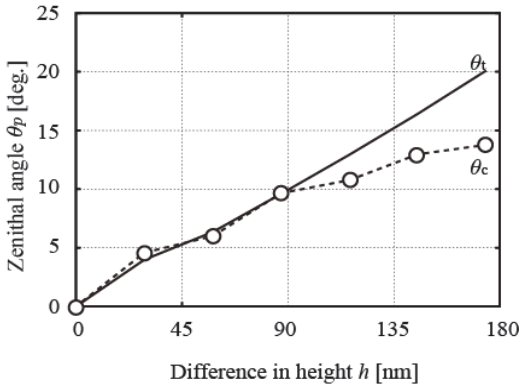

Figure 4: Principal axis angles as function h. Suffixes t and c correspond to analytically and numerically calculated results.

Equation (10) suggests that the orthogonally projected profile of a structure on the xz-plane prevents the overlap with other structures that have different x-coordinate values of the central axis. These are additional conditions of structure dimensions.

2.2 Simulation Results

In this section, we describe the basic characteristics for the proposed method by using numerical analysis. With the proposed method, the distance between a light emitting surface to a light emitting layer is several wavelengths. The wave-optics should be used instead of the geometric optics for analysis in the LED medium. We applied the 3D FDTD method with a perfectly matched layer (PML) boundary condition to verify the control function of the proposed method.

We used InGaN-GaN LEDs as an example. The center wave-length and full width at half maximum (FWHM) of the spectrum were assumed to be 465 and 20 nm, and we ignored the absorption of emitted light in the LEDs. The spectral envelop of emitted light from the LEDs is a Gaussian shape. Therefore, the multiple-dipole sources polarized in the xy-plane is arranged in the light emitting layer and excited with a Gaussian profile in time. For simplicity, the light emitting layer is at 465 nm from the bottom of the structures. The LED and the structures on the light emitting surface were of the same material with index of 2.47 (http://refractiveindex.info/).

The coordinate origin shown in Figure 2 corresponds to the position at the center of the calculation space. The calculation space was 6 μm and accordingly discretized using 15-nm grids. The light emitting layer was distributed inside a circle 930 nm in diameter. The dimensions of the structure were w = 750 nm, p = 930 nm, and b = 750 nm.

First, we discuss the calculated results of the principal axis direction angle θ_p depending on h. Figure 4 shows the direction angles θ_p. In Figure 4, θ_c, indicated with a solid line, was calculated from Equation (4); θ_t, indicated with a dashed line, was obtained from the simulation results. The calculated direction angle θ_c shows the same tendency as θ_t. Below 90nm in h, they are quantitatively the same; above 90nm in h, the increasing tendency of θ_c falls into a sluggish pace compared with θ_t. This is partly because Equation (4) is derived without consideration of aperture shapes. As viewed from θ_p, the shapes of the structure tops are ellipses in $w\cos\theta_p$, which is a minor axis parallel to the x-axis, and the apparent position of structure C moves $h\sin\theta_p$ to the coordinate origin. In this result, a spot of the principal axis is expanded toward -θ, and it limits θ_p.

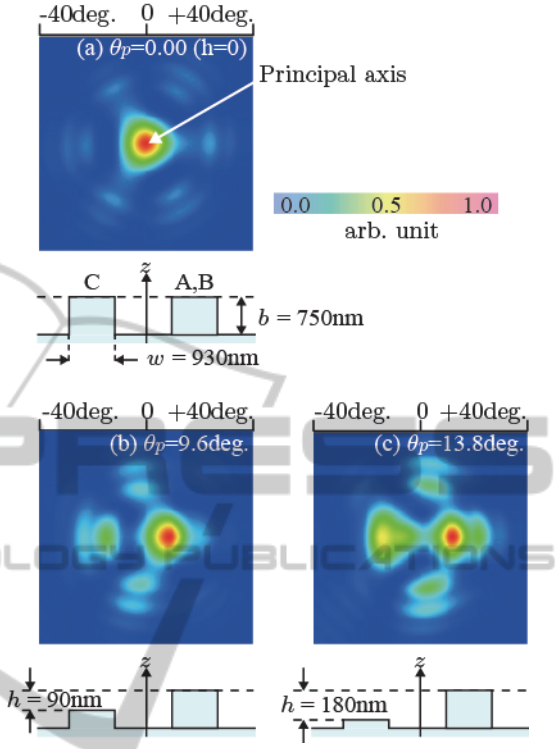

Figure 5: Field intensity distribution corresponding to h = (a) 0, (b) 90 and (c) 180 nm, and cross-section diagram of control unit. Images (a), (b) and (c) were calculated by temporal integration of Poynting vector at 3000 nm from tops of structures. Red and blue regions represent high- and low-intensity parts of field intensity distribution.

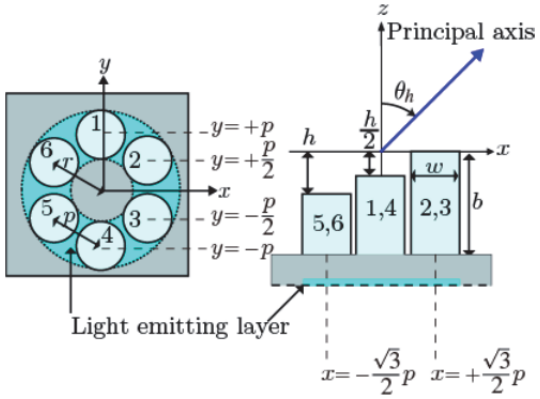

Figure 6: Top view and cross-sectional diagram on vertical plane including x-axis of control unit at N=6.

Next, we discuss the clarity of the principal axis for the proposed method. Figure 5 shows field intensity distribution corresponding to η = 0, 90 and

180 nm. Each image is constructed by temporal integration of a Poynting vector at 3000 nm from the top of the structures. In Figure 5, the high- and low-intensity parts are represented by red and blue regions, respectively. We also show the cross-sectional diagram in a vertical plane. The principal axis direction increases in step with h in Figure 5. The principal axis becomes less clear as h increases. This is because diffraction wave without some kind of stray light affects the field intensity distribution. This is an undesirable characteristic in beaming devices. We discuss a method for obtaining a sharply defined principal axis.

3 IMPROVED STRUCTURE

3.1 Design Rules

In this section, we describe the design rules to improve the clarity of the principal axis based on light use efficiency.

The principal axis consists of lights from the light emitting layer to S via the top of the structures. Other lights, which directly come from the light emitting surface to S, are not involved in forming the principal axis. Thus, a ring-shaped distribution is acceptable as a light emitting layer distribution profile. The inside and outside diameters of the light emitting layer distribution should be equal to those of the inscribed and circumscribed circles of the structures on the light emitting surface.

The light use efficiency of the proposed method is also affected by the number of structures. We estimate the ratio η of light intensity via the tops of N structures to the total amount of light intensity from the light emitting surface. Here, N structures are w in diameter and equally spaced on a circle with a radius r and pitch p. This ratio is expressed as

$$\eta = N\frac{(w/2r)^2}{(1+(w/2r))^2-(1-(w/2r))^2} \tag{11}$$

To calculate η according to Equation (11), we should modify Equation (10) as follows.

$$p\cos\frac{\pi}{6} > w \quad (\mathrm{N}=3) \tag{12}$$

$$p > w \quad (\mathrm{N}=4) \tag{13}$$

$$p\cos\frac{\pi}{6} > w \quad (\mathrm{N}=6) \tag{14}$$

$$p\cos\frac{\pi}{4} > w \quad (\mathrm{N}=8) \tag{15}$$

We then obtain η = 0.325 (N=3), 0.707 (N=4), 0.866 (N=6), and 0.541 (N=8). By comparing these values, we obtain the maximum η at N=6. We can then diminish excess light by using the ring-shaped distribution profile of the light emitting layer and use six structures.

We now describe a modification of Equation (4) for six structures. In this case, r and p are equal. We use p instead of r. Figure 6 shows a single control unit of six structures. For simplicity, structures that have the same x-coordinate value of the central axis are the same height. Then the principal axis direction is described as θ_h. The height of structures 1, 2, 3, 4, 5 and 6 are shown in Figure 6. In this case, optical paths l_k (k = 1 – 6) from the bottoms of structures k to S by way of the tops of the structure are expressed by the following equations.

$$l_1 = l_4 = l + \frac{h}{2}\cos\theta_h \tag{16}$$

$$l_2 = l_3 = l - \frac{\sqrt{3}p}{2}\sin\theta_h \tag{17}$$

$$l_5 = l_6 = l - \frac{\sqrt{3}p}{2}\sin\theta_h + h\cos\theta_h \tag{18}$$

From Equations (16), (17), and (18), the differences in optical path lengths are of three types. First, an optical path length from a pair of structures that are symmetric about the xz-plane is zero in the entire area on the xz-plane. Next, if the x-coordinate value of one of the structures is zero, the optical path length is expressed by the following equation.

$$\frac{\sqrt{3}p}{2}\sin\theta_h - \frac{h}{2}(n-\cos\theta_h) = m\lambda \tag{19}$$

If the signs of the x-coordinate values of structures are opposite, the optical path length is expressed by the following equation

$$\sqrt{3}p\sin\theta_h - h(n-\cos\theta_h) = m\lambda \tag{20}$$

Equations (19) and (20) are equivalent at m=0. We then obtain θ_h by the following equation.

$$\theta_h = \sin^{-1}\frac{nq/2}{\sqrt{1+(q/2)^2}} - \tan^{-1}\frac{q}{2} \tag{21}$$

3.2 Simulation Results

We now explain the simulation results to diminish excess light with the proposed method. To calculate field intensity distribution, we used the 3D FDTD method mentioned in Section 3. The differences with that mentioned in Section 3 are the calculation space size and device structure. The calculation space was 9 μm. The light emitting surface was

covered with a metal mask to obscure light other than from the control unit. The light emitting surface had a hole and the control unit was arranged at the bottom of the hole. Other calculation conditions are listed in Table 1.

Table 1: Calculation conditions.

Diameter of structure (w)	555 nm
Pitch of structures (p)	630 nm
Height of structure (b)	555 nm
Difference in height (h)	0, 90, 180 nm
Outside diameter of light emitting layer	1815 nm
Inside diameter of light emitting layer	705 nm
Depth of light emitting layer from bottoms of structures	465nm
Hole diameter	2325 nm
Metal mask thickness	135 nm

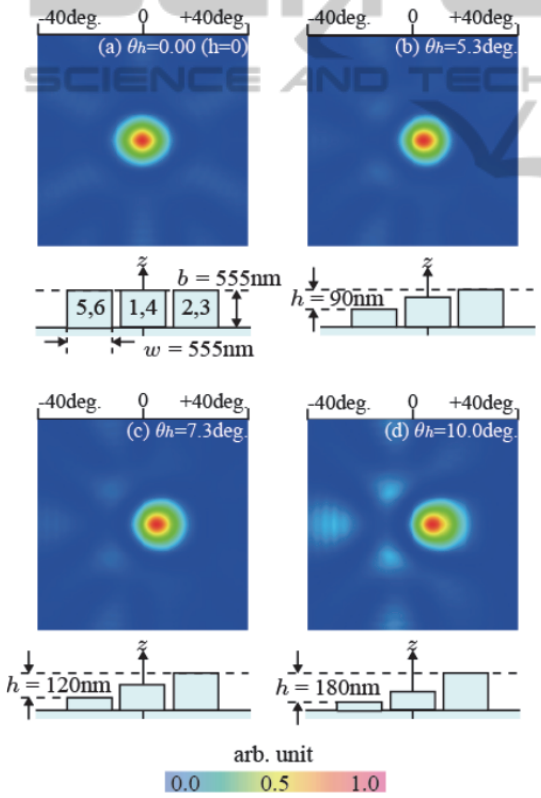

Figure 7: Field intensity distribution of control unit at N=6 corresponding to h = (a) 0, (b) 90, and (c) 180 nm. Images (a), (b), and (c) were calculated by temporal integration of Poynting vector at 5400 nm from tops of structures.

The field intensity distribution corresponded to h = 0 90 and 180 nm. Each image was constructed in the same manner as in Figure 5. However, these images were constructed by the temporal integration of a Poynting vector at 5400 nm from the tops of the structures. Excess light was greatly reduced, as shown in Figure 7. We then obtained a sharply defined principal axis by using the improved proposed method.

4 CONCLUSIONS

We proposed a method for controlling the principal axis direction of LEDs and to obtain a sharply defined principal axis through fine-structures on the light emitting surface. We also verified the effectiveness of the method by using the FDTD method. In this result, a sharply defined principal axis from a 2.3-μm aperture is obtained by using the proposed method.

The proposed method is suitable for high-density array devices because it uses several sub-micron dielectric structures as a means for directional control. By applying the proposed method, high-density beaming array devices are possible. The method is also suitable for ray-based displays or other applications.

We are planning to fabricate a new device with the proposed structure by means of focused ion beam (FIB) technique, which is promising for the fabrication of fine structures with precise control of height as well as in-plane dimension. For the FIB fabrication, the structure and dimension will be designed with FIB's characteristics taking into account. Then, the directional control properties of the new device will be evaluated to verify the effectiveness of the proposed method.

REFERENCES

Krames, M. R., Shchekin, O. B. Mueller-Mach, R., Mueller, G. O., Zhou, L., Harbers, G., and Craford, M., G., 2007, "Status and Futre of High-Power Light-Emitting Diodes for Solild-State Lighting", *IEEE Journal of Display Technology*, 3 (2), 160 - 175. doi:10.1109/JDT.2007.895339.

McKendy, J. J. D., Massoubre, D., Zhang, S., Rae, B. R., Gree, R. P., Gu, E., Henderson, R. K., Kelly, A. E., and Dawson, M. D., 2012, "Visible-Light Communications Using a CMOS-Controlled Micro-Light-Emitting-Diode Array", *IEEE Journal of Lightwave Technology*, 30 (1), 61 - 67. doi:10.1109/JLT.2011.2175090.

Sony Corp., 2012, Sony Develops Next-generation Display, "Crystal LED Display", Ideal for High Picture Quality on Large screens. *Full HD 55-inch Prototype model Exhibited At 2012 International CES*,

News releases of Jan. 10, 2012, Retrieved from: http://www.sony.net/SonyInfo/News/Press/201201/12-005E/

Fournier, F., Rolland, J., 2008, “Design Methodology for High Brightness Projectors”, *IEEE Journal of Display Technology*, 4 (1), 86 - 91. doi:10.1109/JDT.2007.907110.

Tu, S. -H., Pan, J. -W., Wang, C. -M., Lee, Y. -C., and Chang, J. -Y., 2009, “New Collection Systems for Multi LED Light Engines”, *Optical Review*, 16 (3), 318 - 322.

McGroddy, K., David, A., Matioli, E., Iza, M., Nakamura, S., DenBaars, S., Speck, J., S., Weisbuch, C., and Hu, E., L., 2008, "Directional emission control and increased light extraction in GaN photonic crystal light emitting diodes", *Appl. Phys. Lett., 93* (10), 103502. Doi:10.1063/1.2978068.

Lai, C. -F., 2012, Emission aperture size limited the guided mode extraction characteristics of GaN-based ultrathin-film photonic crystal micro-light-emitting diodes, *Appl. Phys. Lett., 101*, 023109. doi: 10.1063/1.4734509.

Son, J. -Y., Javidi, B., Yano, S., and Choi, K. -H., 2010, “Recent Developments in 3-D Imaging Technologies”, *IEEE Journal of Display Technology*, 6 (10), 394 - 403. doi:10.1109/JDT.2010.2045636.

Fattal, D., Pheng, Z., Tran, T., Vo, S., Fiorentino, M., Brug, J., Beausoleil, R. G., 2013, A multi-directional backlight for a wide-angle, glasses-free three-dimentional display, *Nature*, 495, 348-351. Doi:10.1038/nature11972.

Handbook of Optics, 3rd edition, Vol. 4. McGraw-Hill 2009. Retrieved July 30, 2013, from http://refractiveindex.info